https://doi.org/10.1016/j.jnucmat.2014.12.110


# A quantitative phase field model for hydride precipitation in zirconium alloys: Part II. Modeling of temperature dependent hydride precipitation

Zhihua Xiao[1, 2, 3], Mingjun Hao[1,3], Xianghua Guo[4], Guoyi Tang[5] and San-Qiang Shi[1,2,3 *]

[1]The Hong Kong Polytechnic University Shenzhen Research Institute, Shenzhen, China

[2] PolyU Base (Shenzhen) Limited, Shenzhen, China

[3]Department of Mechanical Engineering, Hong Kong Polytechnic University Hung Hom, Kowloon, Hong Kong, China

[4]State Key Laboratory of Explosion and Safety Science, Beijing Institute of Technology, Beijing 100081, China

[5]Advanced Materials Institute, Graduate School at Shenzhen, Tsinghua University, 518055, China

## Abstract

A quantitative free energy functional developed in Part I [1] was applied to model temperature dependent δ-hydride precipitation in zirconium in real time and real length scale. At first, the effect of external tensile load on reorientation of δ-hydrides was calibrated against experimental observations, which provides a quantitative magnification parameter (Mag) for the strain energy in free energy formulation. Then, two types of temperature-related problems were investigated. In the first type, the effect of temperature transient was studied by cooling the Zr-H system at different cooling rates from high temperature while an external tensile stress was maintained. At the end of temperature transients, the average hydride size as a function of cooling rate was

*Corresponding author. E-mail: mmsqshi@polyu.edu.hk.
Tel.: +852 27667821. Fax: +852 23654703.

compared to experimental data. In the second type, the effect of temperature gradients was studied in one or two dimensional temperature field. Different boundary conditions were applied. The results show that the hydride precipitation concentrated at low temperature regimes and that it will eventually lead to the formation of hydride blisters in zirconium. A brief discussion on how to implement the hysteresis of hydrogen solid solubility on hydride precipitation and dissolution in the developed phase field scheme is also presented.

## 1. Introduction

The mechanical strength of metal hydrides is low, which causes great concern about structural integrity [2, 3]. Zirconium alloys are nuclear materials that suffer hydride embrittlement. About 5~20% of hydrogen produced by corrosion will migrate into the alloys. Hydrogen in solid solution diffuses to the tensile region at the flaws if there is a hydrostatic tensile stress gradient, or to the cooler part of materials if there is a temperature gradient. Complicated patterns of hydride precipitates can develop inside the alloys, which may lead to fracture even without an increase of mechanical load. A well-documented example of serious failure occurred in August 1983 in Unit 2 of Pickering A Nuclear Generating Station. In this case, a Zircaloy-2 pressure tube developed an approximately 2 meter long axial crack due to the growth of hydride blisters at points of contact between the pressure tube and the cooler calandria tube surrounding it [4, 5]. Failure due to hydride blisters has been a serious safety concern in other zirconium alloys such as Zircaloy-4 cladding in pressurized light water reactors (PLWR) in countries such as the USA, France and Japan [6-9], and Zr-2.5Nb pressure tubes in pressurized heavy water reactors (PHWR)

in Canada, Argentina, India and South Korea [10-14]. Hydride embrittlement has not only occurred in zirconium alloys, but also in other important metals such as niobium [15], titanium [16], vanadium [17], and more recently in magnesium-aluminum alloy [18, 19], the latter being a candidate in advanced automobile technology.

It is believed that the critical conditions for fracture initiation in hydrides are controlled by the morphology of hydride precipitates in the alloys [20-22]. The morphology of hydride precipitates is controlled by, among other factors, the crystal structure and mechanical properties of hydrides, the orientation of host metal crystals, the temperature distribution, and the orientation and magnitude of the applied stress. The most common hydride in reactor conditions is δ-hydride. It has a face-centered cubic structure as compared to hcp structure of zirconium. It is known that the formation of δ hydrides involves a large volume expansion of about 17% as compared to the original zirconium matrix, resulting in elastic and plastic deformations around the hydrides. Such large elastic and plastic deformations during the formation and dissolution of hydrides are believed to be the reason for a significant hysteresis in hydrogen solid solubility limits found in zirconium [23, 24]. It is also well-known that externally applied stress can cause re-orientation of hydride precipitates.

There are a large number of experimental observations and modelling studies in the literature on hydride precipitation and embrittlement. Nevertheless, a comprehensive, quantitative and multi-dimensional theory that handles all key processes such as hydrogen diffusion, hydride precipitation and fracture under temperature, stress and concentration gradients has not yet been accomplished. Early theoretical investigations considered the process of blister formation using

only the concept of the thermal diffusion of hydrogen [25-27], neglecting the effects of volume changes during hydride formation/dissolution (i.e. elastic and plastic deformation). Recent efforts have included the effects of hysteresis on hydrogen solubility [13, 28, 29], and in some cases researchers have also considered the effects of volume change due to hydrides by evaluating the percentage of hydrides in a given volume [12, 30]. However, these models only estimate hydride volume fraction and cannot predict hydride morphology. Recent progress in phase field modeling of hydride morphology provided a great promise in developing a feasible theoretical and computation scheme that can handle all key processes in multi-dimensional space [31-37], while these studies are at best, still semi-quantitative: quantitative in stress-strain analysis and not quantitative in real time and length scales, or not quantitative in dealing with temperature transient and temperature gradient. Towards developing a comprehensive, quantitative and multi-dimensional phase field model, the Part I of this work [1] was to develop a quantitative description of chemical free energy density and interfacial gradient coefficients that are a function of temperature and other materials parameters. This is a necessary step for a fully quantitative modeling of hydride precipitation. The developed free energy functional was applied to study γ-hydride precipitation in single crystal zirconium after high speed quenching, and the results were compared to TEM observations [38] with reasonable agreement in terms of average hydride size and density [1].

In this work, we will apply the developed free energy functional from Part I [1] to study the effect of temperature on δ-hydride precipitation in zirconium. To the best knowledge of the authors, there is no phase field modeling of δ-hydride in zirconium in the literature, even though the most prevalent hydrides in reactor conditions are δ-hydride. We will first calibrate the

developed model against limited experimental observations. Then, we will study two types of problems related to temperature: the effect of temperature transient and the effect of temperature gradient on δ-hydride precipitation in zirconium.

## 2. **Kinetic equations and quantitative free energy functional for hydride-Zr system**

The kinetic equations in our phase field model are given as follows.

The Cahn-Hilliard diffusion equation with thermal diffusion,

$$\frac{\partial C}{\partial t} = \nabla \cdot \left( M \nabla \frac{\delta F}{\delta C} + \frac{DCQ^*}{RT^2} \nabla T \right) + \xi \tag{1}$$

The Allen-Cahn phase field equation

$$\frac{\partial \eta_p}{\partial t} = -L \frac{\delta F}{\delta \eta_p} + \zeta_p \qquad (p=1, 2, 3\ldots) \tag{2}$$

and the kinetic equation for plastic deformation – an Allen-Cahn type

$$\frac{\partial \varepsilon_{ij}^{pl}}{\partial t} = -N_{ijkl} \frac{\delta E^{dis}}{\delta \varepsilon_{kl}^{pl}} \tag{3}$$

In the above equations, $C$ is hydrogen concentration in the unit of atomic percent, $M$ is the mobility of hydrogen atoms in zirconium, $F$ is the total free energy of the system, $D$ is the chemical diffusion coefficient, $Q^*$ is the heat of transport, $R$ is the gas constant, $T$ is the temperature, $\eta_p$ ($p$ = 1, 2, 3, …) are long range order parameters representing the crystalline variants of the hydride phase, $L$ is a relaxation coefficient, $\xi$ and $\zeta_p$ are noise terms satisfying the fluctuation-dissipation theorem, $\varepsilon_{ij}^{pl}$ are the plastic strains, $E^{dis}$ is the distortion strain energy, $N_{ijkl}$ are kinetic coefficients characterizing the plastic deformation rate, and $t$ is the time.

The total free energy of the Zr-H system is given by

$$F = \int \left[ f(C,\eta_p) + \sum_p \frac{\kappa_p}{2} \left( \nabla \eta_p \right)^2 + \frac{\lambda}{2} \left( \nabla C \right)^2 + Modif \times E \right] dV \tag{4}$$

where $f(C,\eta_p)$ is the local chemical free energy density, $\kappa_p$ and $\lambda$ are interface gradient coefficients, *Modif* is a modification factor that properly accounts for the weighting of the strain energy density $E$ compared to other energy terms in the free energy functional. Ideally, this factor should be 1.0 if all energy terms are completely accurate. While in reality, this is not possible because the theoretical model may never be able to take all possible factors into account. For examples, the real materials may contain various types of defects, impurities, residual stress and so on. Therefore, it may be simpler to introduce the modification factor when using the model to compare with experimental observations. In the above equations, $E$ and $E^{dis}$ are given by [32, 34]

$$\begin{aligned} E = & \frac{1}{2} \int_V C_{ijkl} \varepsilon_{ij}^0(\mathbf{r}) \varepsilon_{kl}^0(\mathbf{r}) d^3r - \frac{1}{2V} C_{ijkl} \int_V \varepsilon_{kl}^0(\mathbf{r}) d^3r \int_V \varepsilon_{kl}^0(\mathbf{r}') d^3r' \\ & - \frac{1}{2} \fint_V \frac{d^3k}{(2\pi)^3} n_i \tilde{\sigma}_{ij}^0(\mathbf{k}) \Omega_{jk}(\mathbf{n}) \tilde{\sigma}_{kl}^0(\mathbf{k})^* n_l - \sigma_{ij}^a \int_V \varepsilon_{ij}^0(\mathbf{r}) d^3r - \frac{V}{2} S_{ijkl} \sigma_{ij}^a \sigma_{kl}^a \end{aligned} \tag{5}$$

$$\begin{aligned} E^{dis} = & \frac{1}{2} \int_V C_{ijkl} e_{ij}^0(\mathbf{r}) e_{kl}^0(\mathbf{r}) d^3r - \frac{1}{2V} C_{ijkl} \int_V e_{kl}^0(\mathbf{r}) d^3r \int_V e_{kl}^0(\mathbf{r}') d^3r' \\ & - \frac{1}{2} \fint_V \frac{d^3k}{(2\pi)^3} n_i \tilde{s}_{ij}^0(\mathbf{k}) \Omega_{jk}(\mathbf{n}) \tilde{s}_{kl}^0(\mathbf{k})^* n_l - s_{ij}^a \int_V e_{kl}^0(\mathbf{r}) d^3r - \frac{V}{2} S_{ijkl} s_{ij}^a s_{kl}^a \end{aligned} \tag{6}$$

where $V$ is the system volume; the integral $\fint$ in infinite reciprocal space is evaluated as a principal value excluding the point $\mathbf{k} = 0$; $\Omega_{jk}(\mathbf{n})$ is the Green function tensor, which is the inverse of the tensor $\Omega_{jk}^{-1}(\mathbf{n}) = n_i C_{ijkl} n_l$; $S_{ijkl}$ is the elastic compliance tensor, which is the inverse to the elastic modulus tensor, $C_{ijkl}$; $\mathbf{n} = \mathbf{k}/k$ is a unit directional vector in reciprocal space; $\tilde{\sigma}_{ij}^0(\mathbf{k}) = C_{ijkl} \tilde{\varepsilon}_{kl}^0(\mathbf{k})$ ; $\tilde{\varepsilon}_{kl}^0(\mathbf{k})$ are the Fourier transforms of $\varepsilon_{kl}^0(\mathbf{r})$ (i.e.,

$\tilde{\varepsilon}_{kl}^{0}(\mathbf{k}) = \int \varepsilon_{kl}^{0}(\mathbf{r}) \cdot \exp(-i\mathbf{k} \cdot \mathbf{r}) d^3 r$ ); the superscript asterisk (*) indicates the complex conjugate; $\sigma_{ij}^{a}$ is the applied external stress; $e_{ij}^{0}(\mathbf{r}) = \varepsilon_{ij}^{0}(\mathbf{r}) - 1/3\varepsilon_{kk}^{0}(\mathbf{r})\delta_{ij}$ are the deviatoric strains, and the deviatoric stress in Fourier space is $\tilde{s}_{ij}^{0}(\mathbf{k}) = \int_V C_{ijkl} e_{kl}^{0}(\mathbf{r}) \exp(-i\mathbf{k} \cdot \mathbf{r}) d^3 r$ . In estimating plastic strains, the von Mises yield criterion is used.

The chemical free energy density was defined in Part I [1] as

$$f(C,\eta_p) = \frac{A_1}{2}(C - C_1)^2 + \frac{A_2}{2}(C_2 - C)\sum_p \eta_p^2 - \frac{A_3}{4}\sum_p \eta_p^4 + \frac{A_4}{6}\sum_p \eta_p^6 + A_5 \sum_{p \neq q} \eta_p^2 \eta_q^2 + A_6 \sum_{p \neq q, q \neq r} \eta_p^4 (\eta_q^2 + \eta_r^2) + A_7 \sum_{p \neq q \neq r} \eta_p^2 \eta_q^2 \eta_r^2 \quad (7)$$

The definitions of $A_1$ to $A_7$, the gradient coefficients ($\kappa_p$ and $\lambda$) and other related parameters are listed in Table 1.

## 3. Parametric study on $\gamma_s$, $\sigma^a$ and *Modif*

In the above quantitative model for H-Zr system, there are a few important parameters that need to be determined. These are: interfacial energy between hydride precipitate and zirconium lattice ($\gamma_s$ ), interfacial energy between two or more hydrides in contact ($\gamma_h$), the interface thickness between a hydride precipitate and the surrounding zirconium lattice or between two or more hydride precipitates in contact ($l$), and the modification factor on strain energy density (*Modif*). Ideally, $\gamma_s$, $\gamma_h$, and $l$ should be determined by theoretical analysis or experimental tests, while *Modif* shall be determined through comparison of the model's predictions with results of hydride nucleation/re-orientation tests under applied stress. To the best knowledge of the authors, there is no well-defined theoretical and experimental results on $\gamma_s$, $\gamma_h$, $l$ and hydride nucleation that can be

directly applied in the current modeling work. Due to the lack of experimental and theoretical data on these parameters in the literature, in Part I of this work [1], it was assumed that $\gamma_s = \gamma_h =$ 0.10 J/m$^2$, $l$ = 0.50 nm, and *Modif* = 4.0, which provided satisfactory modeling results on γ-hydride morphology in single crystal zirconium when compared with an experimental observation. However, these values may not be suitable for δ-hydride modeling because δ-hydrides have a different crystal structure, eigenstrains and H/Zr atomic ratio from that of γ-hydride. Therefore, a parametric study on the effect of $\gamma_s$, $\gamma_h$, *Modif* and applied stress $\sigma^a$ is carried out in the following. Although this parametric study is not conclusive due to the limited availability of suitable theoretical and experimental data that can be used for comparison, it shows the effects that these parameters have on hydride morphology, hence, forming the basis for further studies. Other material properties used in this parametric study are listed in Table 2. In these calculations, the minimum grid size used was 15 nm, the noise terms ($\xi$ and $\zeta_p$) were applied in the first 0.0001 seconds, and plastic deformation was turned on after 0.0015 seconds. All simulations were stopped at 0.003 seconds.

Figure 1 shows the effect that *Modif* and $\sigma^a$ have on δ-hydride morphology at 280ºC under the assumption of $\gamma_s = \gamma_h =$ 0.060 J/m$^2$, $l$ = 0.3 nm, and applied tensile stress in the vertical y-direction. For simplicity, isotropic materials properties are assumed and only three orientations of δ-hydrides in terms of the direction of the hydride platelet normal are considered, i.e., 0º, 60º and 120º relative to the x-direction, respectively. The parameter *Modif* was varied from 1.5 to 1.7 and $\sigma^a$ was varied from 100 to 300 MPa. The following observations can be made. First, the higher is the parameter *Modif*, the less is the number of thermodynamically stable hydrides that form. This is consistent with the conventional nucleation theory according to which the size of a

critical nucleus is proportional to $\frac{\gamma_s}{\Delta g_v - E}$, where $\Delta g_v$ is the chemical free energy density and $E$ is the strain energy density of the body containing the hydride nucleus. For a given undercooling, the effect of increasing *Modif* is to increase $E$, and, therefore the critical size of the hydride nucleus, which means less hydride nuclei will form under the same thermal fluctuation-dissipation conditions ($\xi$ and $\zeta_p$). Second, for the same *Modif*, the increase in applied tensile stress would results in more hydride formation (see cases with *Modif* = 1.5 in Figure 1) because increasing $\sigma^a$ results in a greater negative interaction energy, which reduces $E$ and, hence the size of the critical nucleus. Third, for the same applied stress $\sigma^a$, the higher is *Modif*, the greater is the percentage of hydrides oriented by the uniaxial stress. Increasing *Modif* results in those hydrides not oriented with their largest misfit strain in the applied stress direction to have larger critical sizes for nucleation and hence have a lower probability of forming.

Figure 2 shows the effect of interfacial energy ($\gamma_s$). It is assumed that $\gamma_s = \gamma_h$, $\gamma_s/l = 2\text{x}10^8$ J/m$^3$, *Modif* = 1.6, and applied tensile stress in vertical direction $\sigma^a$ = 250 MPa. It is clear that the increase of interface energy ($\gamma_s$) results in a reduction in number of critical hydride nuclei, which is consistent with predictions of classical nucleation theory. Higher values of $\gamma_s$ would result in more spherically-shaped hydrides instead of the elongated platelet-shaped hydrides observed experimentally. In this model, the interface energy has no direct effect on hydride orientation with or without applied stress, since it was assumed that this energy is isotropic.

## 4. **The effect of cooling rate on δ-hydride morphology**

It should be noted that, because the intent in the following is to study the effect of temperature, and especially a temperature gradient, on hydride morphology, the length scale used in this and in the following section was in the micrometer to millimeter range, which is much larger than the length scale used to obtain the results given in Figure 5 of Part I [1] and in Figures 1 and 2 in this paper. Thus the length scale used is much larger than the sizes of critical hydride nuclei. If one were to choose a nanometer grid size, then the computational time would be very long. Therefore, the minimum grid size in the following work was set at 1 μm, while the sizes of the critical hydride nuclei are of the order of a few to a few tens of nanometers. Therefore, in the following studies, the simulation did not adhere to meeting dictates of the conventional fluctuation-dissipation theorem represented by the two noise terms ($\xi$ and $\zeta_p$) in equations (1) and (2). Instead, a random number generator was used to generate critical hydride nuclei at random locations, while, at the same time, meeting the constraints of mass conservation law in the whole system. With regard to the nucleation rate of critical hydride nuclei for a given simulation condition, such as at a temperature corresponding to a given supersaturation, conventional nucleation rate theory was followed. That is, the nucleation rate for critical hydride nuclei ($\frac{dn}{dt}$) is proportional to $\exp(-\frac{\Delta G^*}{RT}) \times D$ , i.e.,

$$\frac{dn}{dt} \propto \exp(-\frac{\Delta G^*}{RT}) \times D \tag{8}$$

where $\Delta G^*$ is the formation energy of a critically sized nucleus which is inversely proportional to the cube of the undercooling $\Delta T$ . The hydrogen diffusion coefficient $D$ has an exponential dependence on temperature, see Table 2. Since there exist no results of nucleation experiments of the hydride-zirconium system that can establish the nucleation rate as a function of temperature,

we have used in the present simulation classical nucleation rate theory in a relative sense, that is, as expressing the rate in terms of an exponential function of temperature as well as the degree of undercooling $\Delta T$. The actual cooling rates were approximated according to those used in the experiments in reference [39]. The experiments of [39] were done at several different cooling rates from 350°C to about 50°C under a temperature dependent tensile loading ($\sigma^a(MPa) = 594 - 0.5848 \times T(^oC)$). The tensile loading was sufficiently high so that most of the hydride platelets precipitated with their plate edges perpendicular to the tensile loading direction. The average lengths of hydrides and standard deviations at different cooling rates were measured [39]. Unfortunately, the hydride density as a function of cooling rates was not recorded [39]. To compare the results of the present simulation with those of this experiment, we selected a set of simulation parameters for δ-hydrides formation as follows: grid size = 1 μm, $\gamma_s = \gamma_h = 0.060$ J/m$^2$, $l$ = 0.30 nm, *Modfi* = 1.6, and the applied tensile stress following the same function of temperature as in [39]. In practice for simplicity, we actually modeled the cooling process using a step function, that is, the temperature was changed from 350°C to 280°C in the first step, then to 230°C in the second step, then to 180°C in the third step, and so on. The holding time at each temperature step depended on the cooling rate. Our simulation results show that if plastic deformation is applied at the first temperature step (280°C), the hydrides do not grow to plate-like shapes, but end up, instead, as having squared-like shapes. When the plastic deformation is applied at low temperatures, such as at 230°C, then δ-hydrides grow to elongated plate-like shapes as experimentally observed [39]. Figure 3 shows the morphology of δ-hydrides for three cooling rates, in which the plastic deformation was activated at 230°C. On the other hand, when simulating the growth of γ-hydrides using the parameters: grid size = 1 μm, $\gamma_s = \gamma_h = 0.080$ J/m$^2$, $l$ = 0.40 nm, *Modif* = 6, then plastic deformation applied at the high temperature step of 280°C

results in thin needle-shaped hydrides, as shown in Figure 4. Since experimental observations showed that the plate-like δ-hydrides (not squared-like hydrides) form during slow cooling, the above simulation results imply that in real cooling experiments, γ-hydrides may form first with 1:1 atomic ratio between Zr and H, then gradually transform to δ-hydrides at lower temperature with about 1:1.6 atomic ratio between Zr and H. In fact, some experimental [35] and theoretical study [40] have suggested that ζ-hydride with H/Zr ratio less than unity might be the precursor for γ and δ-hydrides during cooling. The ζ-hydride phase has a trigonal symmetry and is fully coherent with hcp α-Zr, resulting in little plasticity during the early stage of growth. Therefore, assuming the absence of plastic deformation at 280°C in Figure 3 may be justified.

## 5. **The effect of temperature gradients on δ-hydride morphology**

Two types of temperature gradients are studied, one is in one dimension (1D) and the other is in two dimensions (2D), given as follows respectively.

$$T = T_1 + (T_2 - T_1)(\cos[(2x/L_x - 1)\pi] + 1)/2 \qquad \text{(for 1D)} \qquad (9)$$

And

$$T = T_1 + \frac{(T_2 - T_1)}{4}(\cos\left[(\frac{2x}{L_x} - 1)\pi\right] + 1) \times (\cos\left[(\frac{2y}{L_y} - 1)\pi\right] + 1) \qquad \text{(for 2D)} \qquad (10)$$

where $L_x$ and $L_y$ are the sizes of the component that experiences the temperature gradients and the minimum grid size in these studies was 4 μm. The temperature distributions are shown in Figure 5 and 6.

For simplicity, we assume that the platelet normal of all δ-hydrides is perpendicular to the paper plane. The initial hydrogen concentration $C_o$ = 0.5 at%. The boundary conditions at high temperature is kept at $C_H$ = 0.5 at% to maintain a constant level of hydrogen. At the beginning of the simulations, random δ-hydride seeds are generated at the cold region of the field where the temperature is such that terminal solid solubility of hydrogen for hydride precipitation (TSSP) is exceeded. The evolution of hydride morphologies under these 1D and 2D temperature gradients are presented in Figures 7 and 8, respectively. As can be seen from these figures, hydrides at the cold region will grow as a function of time. With time and an inexhaustible supply of hydrogen at the hot boundary, the sizes of the hydrides at the cold region will increase continuously, leading to the formation of a hydride blister at the cold spot.

The calculations presented in this paper demonstrates that the developed quantitative phase field method can be used to predict, for the first time, hydride or hydride blister formation under temperature, concentration, and stress gradients.

## 6. Discussion on inclusion of hysteresis of hydrogen solid solubility in future PFM formulations

When dealing with the effect of temperature on hydride precipitation or dissolution in zirconium alloys, especially when a temperature cycling is involved as it is in almost all practical cases, it is important that the model can handle the considerable hysteresis in the terminal hydrogen solid solubility adequately. The hysteresis in the terminal solid solubility of hydrogen in Zr-H systems is illustrated in Figure 9. It shows that for a given hydrogen concentration in solid solution in

zirconium, the temperature at which hydrides start to precipitate during cooling (TSSP line, here arbitrarily choosing one experimentally determined by Slattery [41]) can be as much as 50$^{o}$C lower than that for hydride dissolution temperature during heating (TSSD line, here arbitrarily showing one experimentally determined by Kearns [42]). Equivalently, at a given temperature, the hydrogen concentration in solid solution required for hydride precipitation is greater than that for hydride dissolution. The left lower corner (left to Kearns' line) in Figure 9 represents the condition at which all hydrogen atoms are in solid solution, while the top right corner (right to Slattery's line) in Figure 9 indicates that hydrides are present. In the region between Kearns' line (TSSD) and Slattery's line (TSSP), the stable phase(s) should depend on the immediate thermal history (cooling or heating): hydrides will be present if the temperature is reached from a temperature lower than the TSSP line; or all hydrogen atoms are in solid solution if the temperature is reached by cooling down from a temperature higher than the TSSD line. The locus of points given by the TSSP line in Figure 9 indicates the temperature for a given hydrogen content at which the first hydride is formed in the solid during cooling, while the locus of points given by the TSSD line in Figure 9 represents the temperature for a given total hydrogen content at which the last hydride has dissolved in the solid during heating. These lines are also referred to as phase field boundaries. In incoherent equilibrium these lines would coincide, there would be no hysteresis, and they would also be representative of the tie-line compositions; i.e., the compositions of the two phases in equilibrium remain the same for a given temperature regardless of the phase fraction of the two phases. The combination of phase field and tie-line compositions is often also loosely referred to as the solvus compositions. When there are coherency strains between the two phases the lie-line compositions vary with phase fraction of the two phases or total hydrogen content. This variation in composition with phase fraction may

not, however, by itself lead to hysteresis. In a system for a temperature range where one component is much more mobile than the other, e.g., hydrogen versus zirconium, respectively, phase transformation can occur rapidly while not all, or any, of the misfit strains between the two phases (hydride and $\alpha$-Zr) are relieved. Partial relieve of the misfit strains can occur in this case through plastic deformation once hydride precipitates have reached a sufficient size during precipitation and dissolution. The plastic work produced is non-recoverable and has been suggested as one source of hysteresis [43]. In addition, Flanagan et al [44] have proposed as another source of hysteresis that in phase transformations involving coherency strains between the phases, the resultant energy barrier is a finite one that cannot be overcome by microscopic composition fluctuations at constant temperature. A finite driving force is needed such as a finite decrease or increase in temperature, to overcome this barrier. The application of such a finite driving force results in a finite increase or decrease of the minority phase. This finite transfer of matter results in entropy production, which forms another possible source for hysteresis between hydride formation and dissolution. Thus equilibrium between the two phases is not possible in this case, although a reference, incoherent two-phase equilibrium state can be defined for applications to models where such an equilibrium state is needed. In most cases deriving an expression for this reference state involves deriving a theoretical estimate of the reference incoherent equilibrium state, from the experimental data affected by hysteresis. A recent book by Puls [45] had provided a comprehensive and in depth discussion on hysteresis and related issues.

The effect of hysteresis shall be included in the model in order to properly predict the hydride morphology if a temperature cycling is involved. To fulfill this task, one needs to develop a

single-well free energy functional for the left lower corner region of Figure 9 with the well minimum located at the average concentration of hydrogen. The exact form of such a free energy functional is not important, as long as it predicts hydride dissolution when the TSSD line is crossed from the hydride side, and the equilibrium concentration of hydrogen in solid solution ($C_\alpha$) should be equal to the average hydrogen concentration ($C_o$) in the system. While at the top right corner region of Figure 9, the double-well free energy functional developed in this work (Part I and II) should be applied.

## 7. Conclusion

A quantitative, elastoplastic phase field model developed in Part I [1] is applied to study the evolution of δ-hydride and γ-hydride precipitation in zirconium under stress and/or temperature gradients in real time and real length scale. With a proper application of TSS data, the model is capable to handle temperature transients as well as temperature gradients. The results also demonstrate that some of the materials properties are important in controlling hydride morphology, such as interfacial energy of hydrides and hydride nucleation rate as a function of temperature as well as hydrogen supersaturation, which are not available from the literature. All simulations presented here are in two dimensional to reduce the computational time, while the theoretical framework and methodology developed are suitable for three dimensional analysis.

The authors would like to thank Dr. Manfred P. Puls for valuable comments on the manuscript. This work was supported by grants from the Research Grants Council of Hong Kong (PolyU

5267/10E), from the National Natural Science Foundation of China (No.51271157) and from Shenzhen government fundamental research fund (JC201104220351A).

**References**

[1] S.Q. Shi and Z.H. Xiao, "A quantitative phase field model for hydride precipitation in zirconium alloys: Part I. Development of quantitative free energy functional", Journal of Nuclear Materials, published on line on March 6, 2014.

[2] R. Dutton, The Metallurgical Society of CIM Annual Volume, 1978, pp.16.

[3] H.K. Birnbaum, in Hydrogen Effects on Material Behavior, edited by N.R. Moody and A.W. Thompson, 1989, pp. 639.

[4] A. Sawatzky, Canadian Metallurgical Quarterly, vol. 24, issue 3, July 1985, pp. 217-223.

[5] B.A. Cheadle, C.E. Coleman and J.F.R. Ambler, ASTM STP 939, R.B. Adamson and L.F.P. Van Swam, Eds., ASTM, Philadelphia, 1987, pp. 224-240.

[6] A.M. Garde, G.P. Smith, R.C. Pirek, in Zirconium in the Nuclear Industry: Eleventh International Symposium, ASTM STP 1295, edited by G.P. Sabol, American Society for Testing and Materials, Philadelphia, PA, 1996, pp. 407-429.

[7] J.B. Bai, C. Prioul, D. Francois, Metall. Mater. Trans. A, 25A, 1994, pp.1185.

[8] H.M. Chung and T.F. Kassner, Nuclear Engineering and Design, vol. 186, 1998, pp.411-427.

[9] O.N. Pierron, D.A. Koss, A.T. Motta, K.S. Chan, J. Nucl. Mater., vol. 322, 2003, pp. 21-35.

[10] M. Leger, T.P. Byrne, A.C. Wallace, D.V. Leemans, Ont. Hydro Res. Rev. No. 8, 1993, pp. 46.

[11] G. Domizzi, R.A. Enrique, J. Ovejero-Garcia, G.C. Buscaglia, Journal of Nuclear Materials, vol. 229, 1996, pp. 36.

[12] D.R. Metzger, R.G. Sauve, T.P. Byrne, ASME Pressure Vessels and Piping Division, vol. 2006, pp. 8.

[13] R.N. Singh, R. Kishore, T.K. Sinha, B.P. Kashyap, J. Nucl. Mater., vol. 301, 2002, pp.153.

[14] Y.J. Kim, S.L. Kwak, J.S. Lee and Y.W. Park, KSME International Journal, vol. 17, Issue 7, 2003, pp.947-957.

[15] H. Mastsui, N. Yoshikawa and M. Koiwa, Acta Metall., vol. 35, 1987, pp. 413.

[16] H.Z. Xiao, S.J. Gao and X.J. Wan, Scr. Metall., vol. 21, pp. 265.

[17] S. Takano and T. Suzuki, Acta. Metall., vol. 22, 1974, pp. 265.

[18] N. Winzer, A. Atrens, W. Dietzel, G. Song, K.U. Kainer, Materials Science and Engineering A, vol. 466, issue 1-2, 2007, pp.18-31.

[19] N. Winzer, A. Atrens, W. Dietzel, G. Song, K.U. Kainer, Advanced Engineering Materials, vol.10, Issue 5, 2008, pp. 453-458.

[20] R.L. Eadie, D.R. Metzger and M. Leger, Scr. Metall., vol. 29, 1993, pp. 335.

[21] S.Q. Shi and M.P. Puls, J. Nucl. Mater., vol. 208, 1994, pp. 232.

[22] S.Q. Shi, M.P. Puls and S. Sagat, J. Nucl. Mater., vol. 208, 1994, pp. 243.

[23] B.W. Leitch and S.Q. Shi, Modeling and Simulation in Materials Science and Engineering, Vol. 4, pp. 281-292, 1996.

[24] S.Q. Shi, G.K. Shek and M.P. Puls, J. Nucl. Mater., Vol. 218, pp. 189-201, 1995.

[25] A. Sawatzky, J. Nucl. Mater. 2 (1960) 62.

[26] J.M. Markowitz, Trans. Metall. Soc. AIME 221 (1961) 819.

[27] A. Sawatzky and E. Vogt, Trans. Metall. Soc. AIME 227 (1963) 917.

[28] T.P. Byrne and M. Leger, Ontario Hydro Research Division, Report 85-29-H (1985).

[29] M. Leger and T.P. Byrne, Proceedings of the 12th Conference on Simulation Symposium on Reactor Dynamics and Plant Control, Hamilton, Canada, April 1986.

[30] A.G. Varias and A.R. Massih, Eng. Fract. Mech., vol. 65, 2000, pp. 29.

[31] X.Q. Ma, S.Q. Shi, L.Q. Chen and C.H. Woo, Computational Materials Science, 23 (2002) 283~290.

[32] X.H. Guo, S.Q. Shi, Q.M. Zhang, X.Q. Ma, J. Nucl. Mater. 378 (2008) 110.

[33] X.Q. Ma, S.Q. Shi, C.H. Woo and L.Q. Chen, Scripta Materialia, 47 (2002) 237~241.

[34] X.H. Guo, S.Q. Shi, Q.M. Zhang, X.Q. Ma, J. Nucl. Mater. 378 (2008) 120.

[35] Z. Zhao et al. J. ASTM Int. 5 (2008) Paper ID JAI101161.

[36] L. Thuinet, A. De Backer, A. Legris, Acta Materialia 60 (2012) 5311–5321.

[37] L. Thuinet, A. Legris, L. Zhang, A. Ambard, Journal of Nucl. Mater. 438 (2013) 32–40.

[38] J.E. Bailey, Acta Metal. 11 (1963) 267.

[39] S.Q. Shi and M.P. Puls, Journal of Nuclear Materials, 275 (1999) 312-317.

[40] L. Thuinet and R. Besson, Intermetallics, 20 (2012) 24-32.

[41] G.F. Slattery, J. Inst. Metals, 95 (1967) 43-47.

[42] J.T. Kearns, J. Nucl. Mat., 22 (1967) 292.

[43] H.K. Birnbaum, M.L. Grossbeck and M. Amano, J. Less-Common Metals**,** 49 (1976) 357.

[44] T.B. Flanagan and J.D. Clewley, J. Less-Common Metals, 83 (1982) 127.

[45] M.P. Puls, The Effect of Hydrogen and Hydrides on the Integrity of Zirconium Alloy Components, Springer, 2012, ISBN 978-1-4471-4195-2.

**Table 1. Definitions of parameters in chemical free energy density and gradient coefficients**

---

$A_1 = 2\Delta g$

$A_2 = 4\Delta g(C_2 - C_1)$

$A_3 = A_4 = 12[\Delta g(C_2 - C_1)^2 - f(C_2, \pm 1)]$

$A_5 = A_6 = A_7 = \frac{3}{2}\left[\frac{\gamma_h}{l} + \frac{11}{420}A_3 - \frac{2\kappa_p}{l^2}\right]$

$\kappa_p = \lambda(C_\beta - C_\alpha)$

$\lambda = \frac{\gamma_s^2}{4(C_\beta - C_\alpha)^4 I^2 \Delta g}$

$\frac{\gamma_s}{l} = 2(C_\beta - C_\alpha)^2 \Delta g \cdot I\sqrt{1 - \frac{5}{16}(1-a) - a}$

$\gamma_s$ : interface energy between zirconium lattice and a hydride

$\gamma_h$ : interface energy between two hydrides in contact

$l$ : interface thickness

$I = \int_0^1 \left\{3\eta^2 - 2\eta^3 - 12\left[\frac{1}{4} - \frac{1}{6}\eta^2\right]\eta^4[1-a] - a\eta\right\}^{1/2} d\eta$

$f(C_2, \pm 1) \approx (C_\beta - C_\alpha)\frac{RT}{V_\alpha}\ln\frac{C_\alpha}{C_1}$

$C_1 \approx C_\alpha \exp\left[\frac{\gamma_s}{l} \cdot \frac{V_\alpha}{RT(C_\beta - C_\alpha)}\right]$

$C_2 \approx C_\beta \exp\left[\frac{\gamma_s}{l} \cdot \frac{V_\alpha}{RT(C_\beta - C_\alpha)}\right]$

$$\Delta g \approx \frac{RT}{V_\alpha \cdot a \cdot (C_\beta - C_\alpha)} \ln \frac{C_\alpha}{C_1} = -\frac{\gamma_s}{l} \cdot \frac{1}{a\left(C_\beta - C_\alpha\right)^2}$$

The parameter *a* is a weak function of temperature at reactor operating conditions [1].

---

**Table 2. Material properties used in modeling of δ-hydrides in zirconium**

---

$\frac{\gamma_s}{l} = 2\times10^8\ J/m^3$

$V_\alpha = 1.67\times10^{-6}\ m^3/mol$

$D = 7.73\times10^{-7}\ \exp(-45300/RT)\ m^2/s$

$A_5 = 0.08A_3$

$Q^* = 20930$ J/mol

$R = 8.314\ J/mole\ K$

Yield stress = 1088 – 1.02T(K) MPa for unirradiated materials

Yield stress = 1388 – 1.02T(K) MPa for irradiated materials

Young's modulus = 95900 – 57.4{T(K) - 273} MPa

Poisson ratio = $0.436 - 4.8\times10^{-4}$ {T(K) – 300}

TSSP(at%) = $C_\alpha = 3.75\exp(-28000/RT)$

TSSD(at%) = 5.53exp(-33300/RT)

Eigenstrains of hydrogen interstitials in Zr: $\varepsilon_{11} = \varepsilon_{22} = 0.0329$, $\varepsilon_{33} = 0.0542$.

Eigenstrains of γ-hydride in Zr: 0.00551, 0.0564 and 0.0570 in $[11\bar{2}0]$, $[1\bar{1}00]$ and $[0001]$ direction, respectively.

Eigenstrains of δ-hydride in Zr: 0.0458, 0.0458 and 0.072 in $[11\bar{2}0]$, $[1\bar{1}00]$ and $[0001]$ direction, respectively.

---

**Figures**

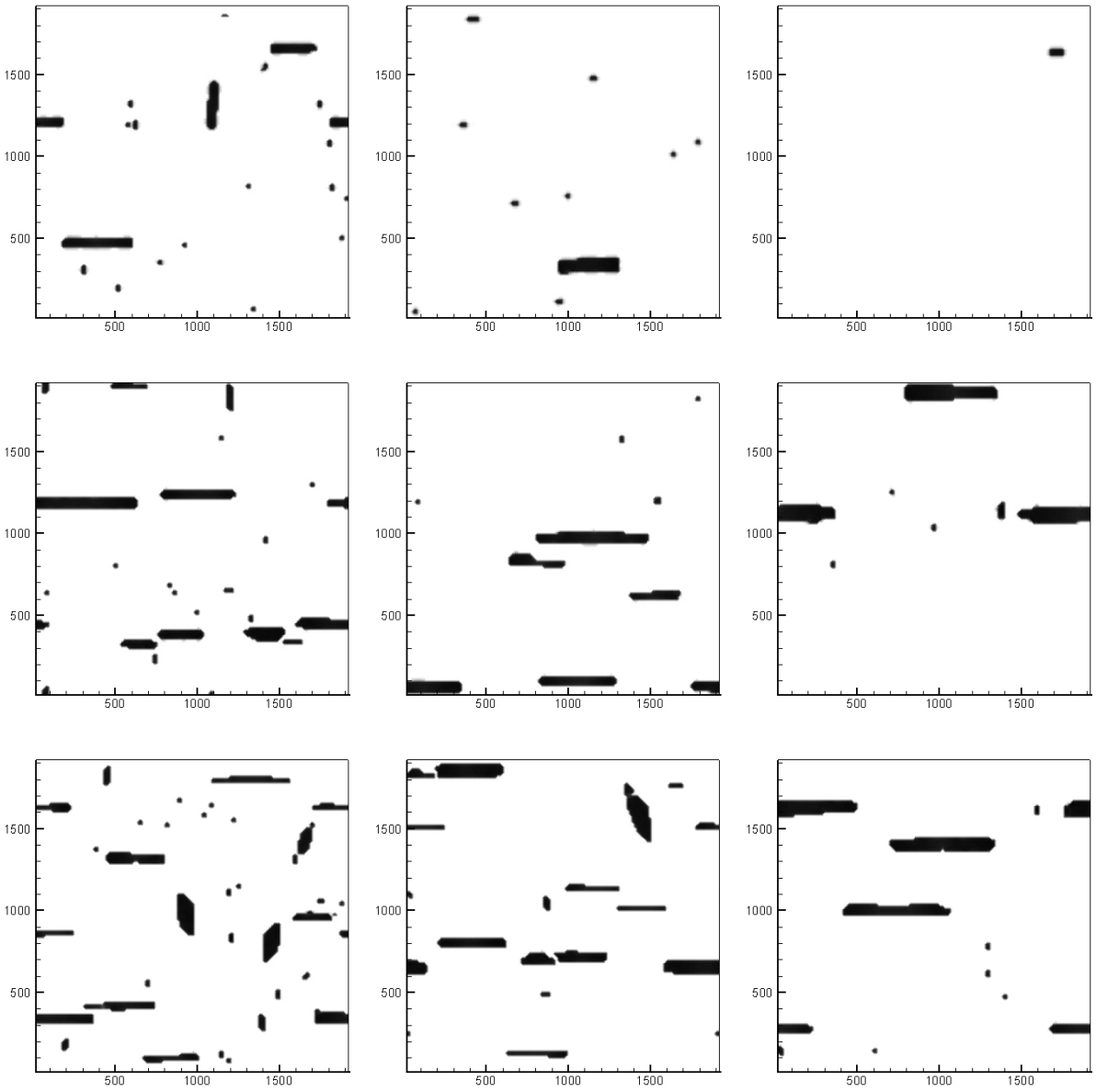


Figure 1. Effect of *Modif* and $\sigma^a$ on δ-hydride morphology. The initial hydrogen concentration $C_o$ = 0.9 at%, and temperature is at 553K. Grid size = 15 nm, and the units of x and y axis are in nm. $\gamma_s = \gamma_h$ = 0.060 J/m$^2$, $l$ = 0.30 nm, the applied tensile stress is in vertical direction. The first row: $\sigma^a$ = 100MPa; the second row: $\sigma^a$ = 200MPa; and the third row: $\sigma^a$ = 300MPa. The first column: *Modif* = 1.5; the 2$^{nd}$ column: *Modif* = 1.6; and 3$^{rd}$ column: *Modif* = 1.7.

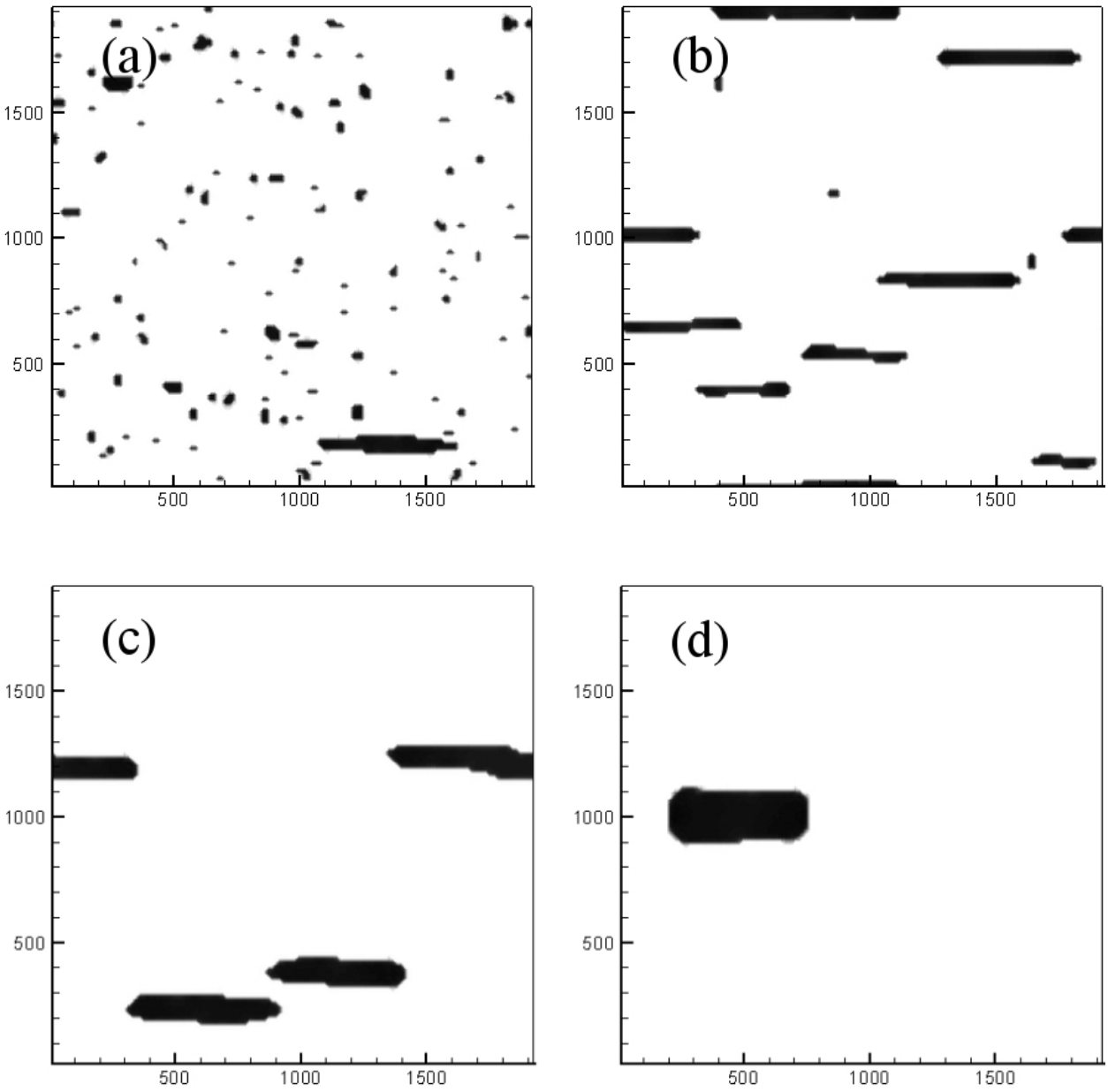


Figure 2. Effect of interfacial energy ($\gamma_s$). The initial hydrogen concentration $C_o$ = 0.9 at%, and temperature is at 553K. Grid size = 15 nm, and the units of x and y axis are in nm. It is assumed that $\gamma_s = \gamma_h$, $\gamma_s/l = 2\text{x}10^8$ J/m$^3$, *Modif* = 1.6, and applied tensile stress in vertical direction $\sigma^a$ = 250 MPa. (a). $\gamma_s$ = 0.05 J/m$^2$; (b). $\gamma_s$ = 0.06 J/m$^2$; (c). $\gamma_s$ = 0.07 J/m$^2$; and (d). $\gamma_s$ = 0.08 J/m$^2$. There is no stable hydride when $\gamma_s \geq 0.09$ J/m$^2$.

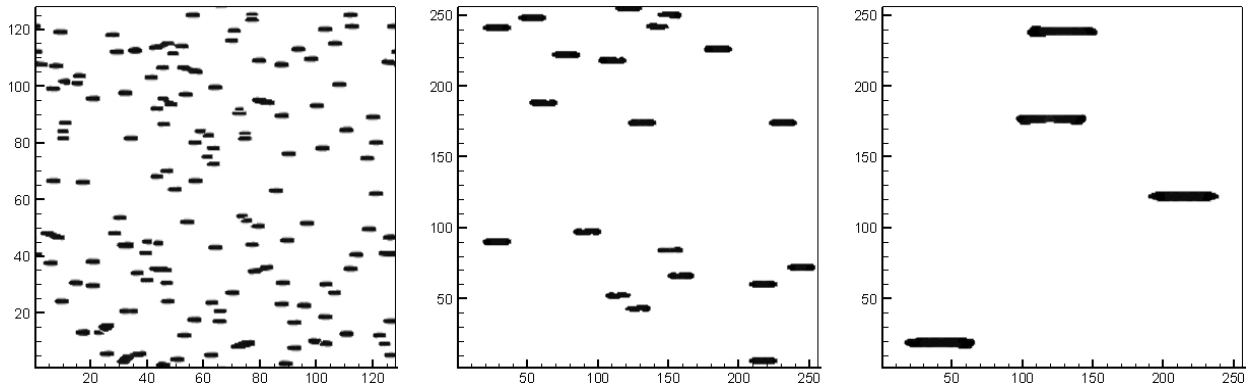


Figure 3. Simulation results on δ-Hydride morphology under different cooling rates. The cooling process was from 350ºC to about 50ºC under applied tensile stress in Y-direction [39]. The grid size is 1 μm. The average hydrogen concentration $C_o$ = 0.9 at% (100 ppm wt%), $\gamma_s$ = 0.060 J/m$^2$, $l$ = 0.30 nm, and $Mag$ = 1.6. From left to right, the cooling is completed in 0.07 hours, 2.5 hours, and 6 hours, respectively. The units of x and y axis are in μm. The plastic deformation was applied at 230ºC.

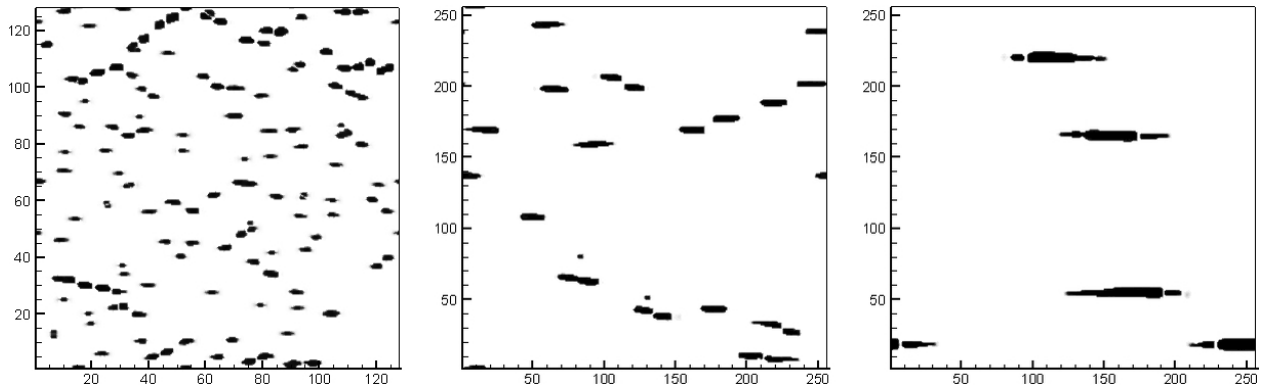


Figure 4. Simulation results on γ-Hydride morphology under different cooling rates. The cooling process was from 350°C to about 50°C under applied tensile stress in y-direction [39]. The grid size is 1 μm. The average hydrogen concentration $C_o$ = 0.9 at% (100 ppm wt%), $\gamma_s$ = 0.080 J/m$^2$, $l$ = 0.40 nm, and $Mag$ = 6. From left to right, the cooling is completed in 0.07 hours, 2.5 hours, and 6 hours, respectively. The units of x and y axis are in μm. The plastic deformation was applied at 280°C.

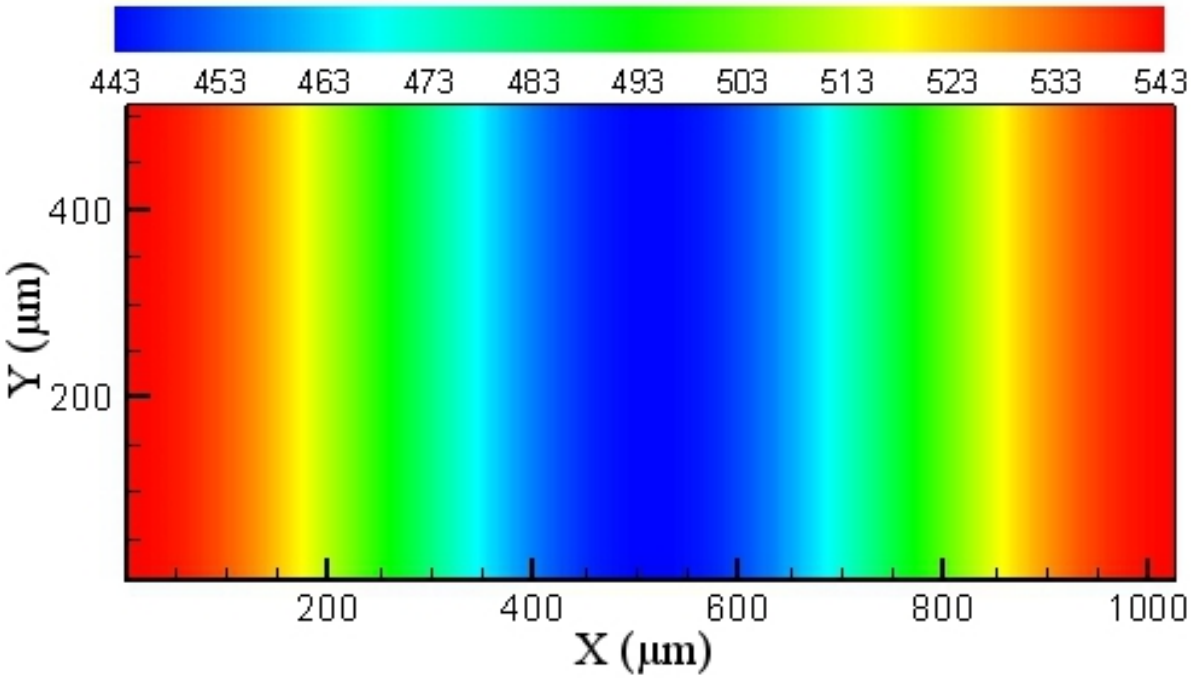


Figure 5. The 1D temperature distribution. The unit of temperature is in Kelvin.

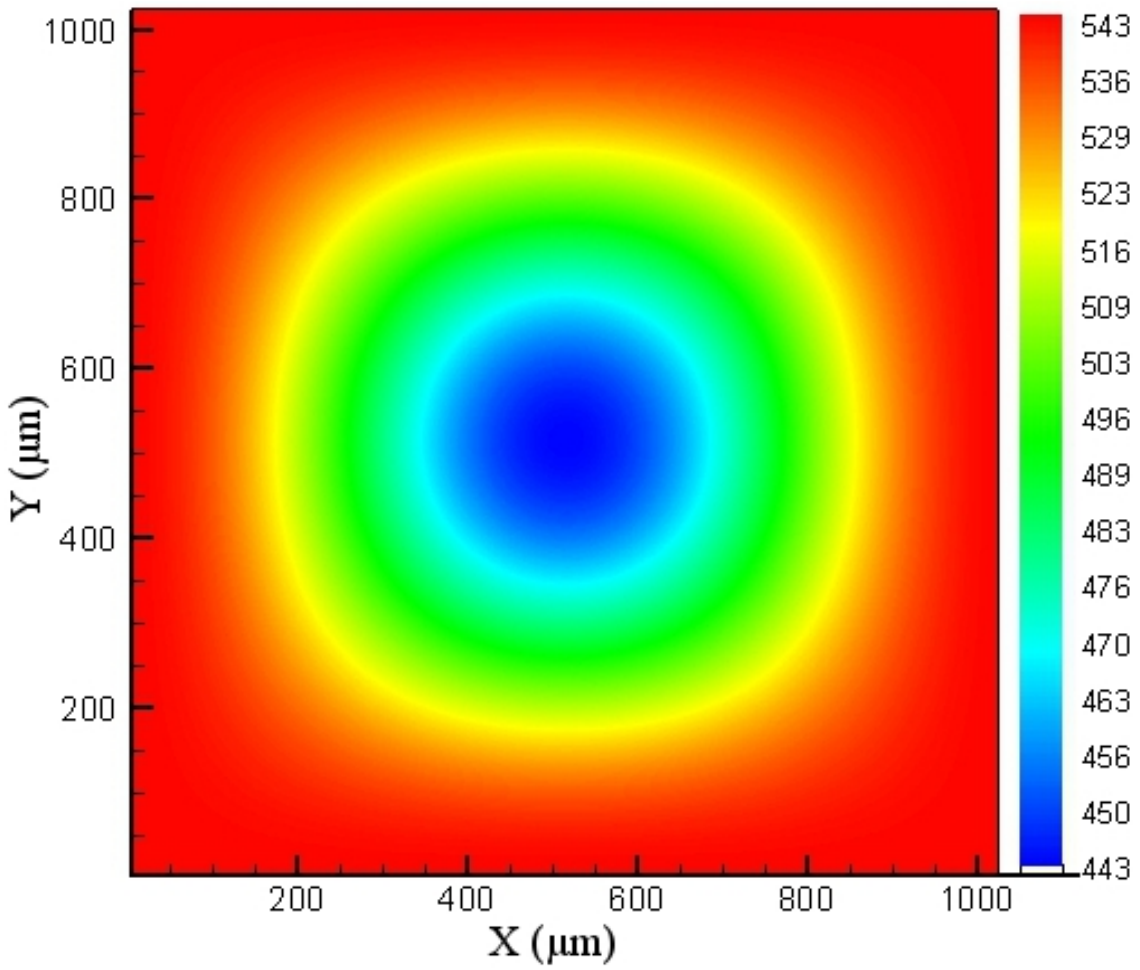


Figure 6. 2D temperature field. The unit of temperature is in degree Kelvin.

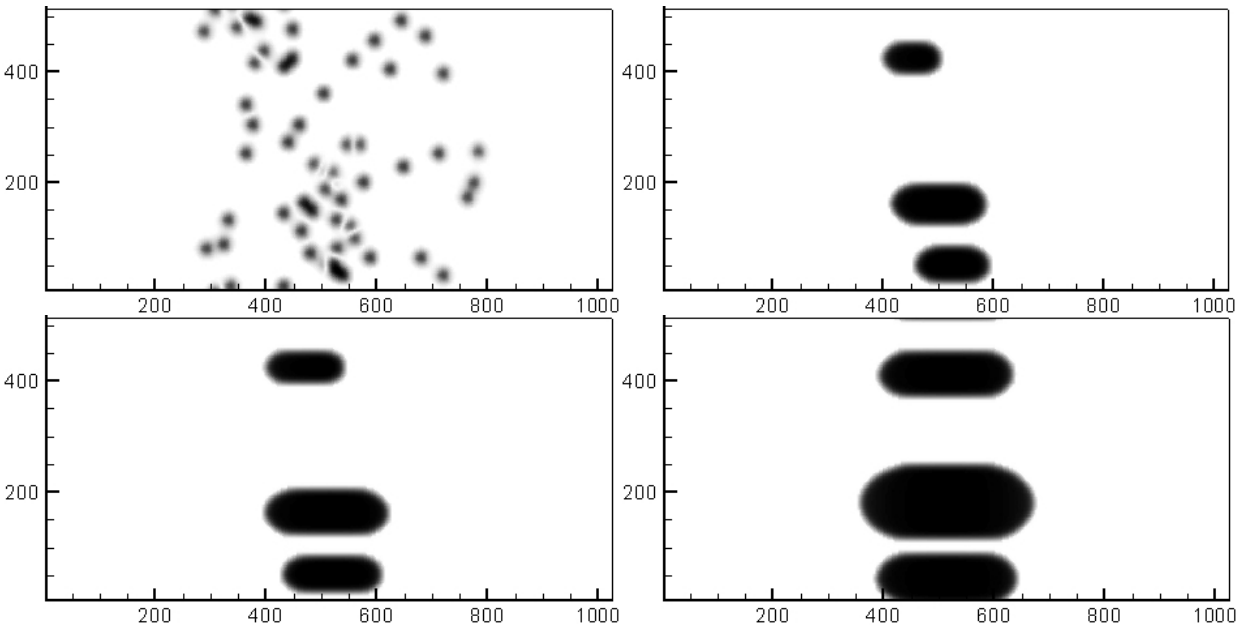


Figure 7. δ-hydride morphology in 1D temperature gradient as a function of time. The grid size is 4 μm. The units of x and y axis are in μm. Initial condition: $C_o$ = 0.5 at%; boundary condition at left and right boundaries: $C_H$ = 0.5 at%; $\gamma_s$ = 0.012 J/m$^2$, $l$ = 0.60 nm, and $Mag$ = 4. (a). t = 1.5 sec; (b). t = 750 sec; (c). t = 1500 sec; (d). t = 4500 sec.

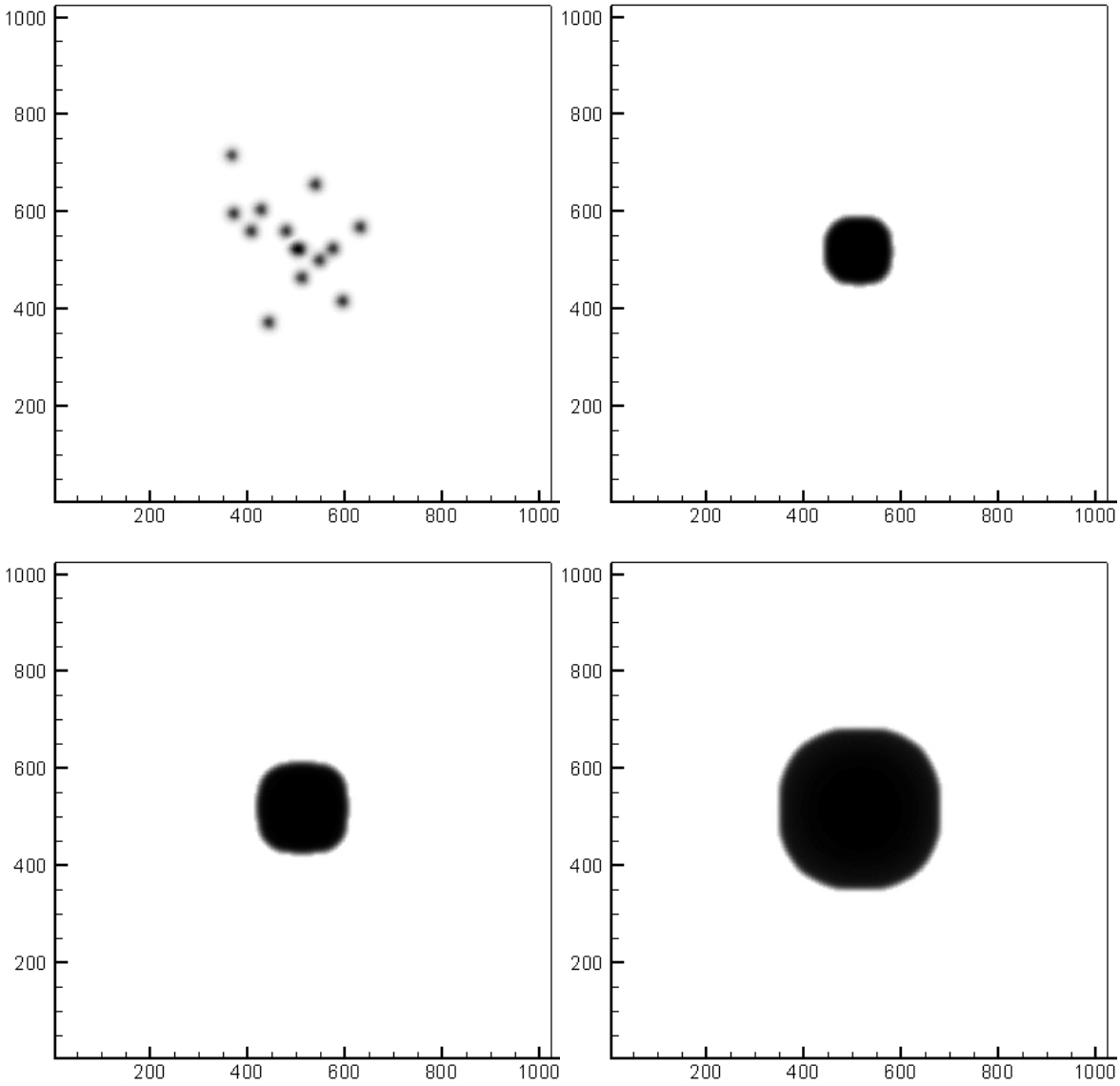


Figure 8. $\delta$-hydride distribution in 2D temperature gradients. Hydride platelets are assumed to be parallel to the 2D plane. The grid size in simulations is 4 μm. The units of x and y axis are in μm. Initial condition: $C_o$ = 0.5 at%; boundary condition at all four boundaries: $C_H$ = 0.5 at%; $\gamma_s$ = 0.012 J/m$^2$, $l$ = 0.60 nm, and $Mag$ = 4. (a). t = 1.5 sec; (b). t = 750 sec; (c). t = 1500 sec; (d). t = 4500 sec.

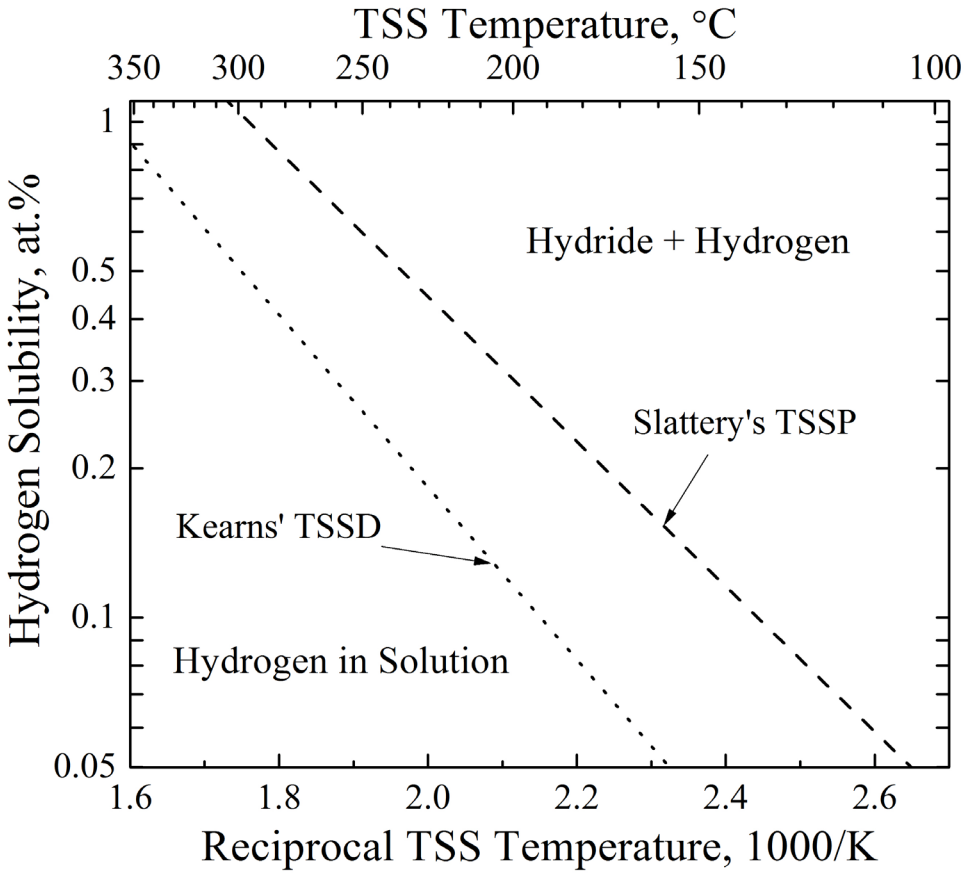


Figure 9. The hysteresis of hydrogen solid solubility in zirconium.